LETTER • OPEN ACCESS

Synchrony in directed connectomes

To cite this article: J. J. Crofts *et al* 2022 *EPL* **139** 42004

A Letters Journal Exploring the Frontiers of Physics

August 2022

EPL, **139** (2022) 42004
doi: 10.1209/0295-5075/ac8176

www.epljournal.org

Synchrony in directed connectomes

J. J. Crofts[a], N. Chuzhanova, A. Padmore and M. R. Nelson

Nottingham Trent University, School of Science and Technology - Nottingham, NG11 8NS, UK

received 18 December 2021; accepted in final form 15 July 2022
published online 16 August 2022

Abstract – Synchronisation plays a fundamental role in a variety of physiological functions, such as visual perception, cognitive function, sleep and arousal. The precise role of the interplay between local dynamics and directed cortical topology on the propensity for cortical structures to synchronise, however, remains poorly understood. Here, we study the impact that directed network topology has on the synchronisation properties of the brain by considering a range of species and parcellations, including the cortex of the cat and the Macaque monkey, as well as the nervous system of the *C. elegans* round worm. We deploy a Kuramoto phase model to simulate neural dynamics on the aforementioned connectomes, and investigate the extent to which network directionality influences distributed patterns of neural synchrony. In particular, we find that network directionality induces both slower synchronisation speeds and more robust phase locking in the presence of network delays. Moreover, in contrast to large-scale connectomes, we find that recently observed relations between resting state directionality patterns and network structure appear to break down for invertebrate networks such as the *C. elegans* connectome, thus suggesting that observed variations in directed network topology at different scales can significantly impact patterns of neural synchrony. Our results suggest that directionality plays a key role in shaping network dynamics and moreover that its exclusion risks simplifying neural activation dynamics in a potentially significant way.

Introduction. – Over the past two decades, network science has had a profound impact on the study of complex systems arising throughout the social and natural sciences, communication and information technologies and information sciences [1,2]. A defining feature of such systems is their ability to synchronise; that is, for their nodal dynamics to align (or become entrained) over time through an intricate interplay between local dynamics and structural connectivity [3,4]. Neuroscience, in particular, contains a plethora of examples of such synchrony, which can be both advantageous (*e.g.*, control of motor systems [5]) and detrimental (*e.g.*, Parkinson's disease or epileptic seizures [6,7]) to the functioning of such neural systems.

Questions of synchronisation are thus of particular importance in neuroscience, with coherent oscillations between distant brain structures proposed as a mechanism for the propagation behaviour of neural activity [8], which is commonly manifested via functional connectivity of the brain [9]. Modelling approaches that deploy biologically realistic connectivity data, obtained from modern non-invasive structural brain imaging methodologies, have been successfully used to probe synchronisation phenomena related to oscillatory brain rhythms in both healthy and diseased brains [10–13]. Such studies, however, predominantly treat the connectome (*i.e.*, the wiring diagram describing an organism's nervous system) as an undirected network, largely due to the inability of imaging techniques to infer directionality of neural signals. Thus, the question of how the directed topological structure of connectome-based networks impacts mechanisms underlying synchronisation phenomena is far from understood, despite a small number of recent studies [14,15] highlighting the significant impact of network directionality in subserving network dynamics. In particular, it is largely unknown whether or not directed topology enhances or destabilises synchrony in the brain, or indeed, what effect it has on the speed of synchronisation, and moreover the role that time delays play when directionality is incorporated.

[a]E-mail: jonathan.crofts@ntu.ac.uk (corresponding author)

In this letter we address these questions by simulating neural dynamics on connectome-based networks for a range of species and parcellations that contain directionality information. Neural activity is described by a phase-delayed Kuramoto Model (KM), which is perhaps the simplest example of a delay-coupled oscillatory network [16] and is thus well suited to assessing how directed connectomes govern synchronisation properties of the brain [17]. Our results highlight the important role directionality plays in determining observed patterns of phase synchronisation within both large- and micro-scale cortical networks. In particular, we find that large-scale mammalian connectomes appear to form a distinct family of networks as characterised by their synchrony properties, whilst the micro-scale invertebrate network of *C. elegans* does not appear to fit within this classification, due to variations in the directed network topology between these networks.

Methods. –

Cortical networks. To investigate the impact of directionality on the synchronisation properties of connectome-based networks we consider a variety of different organisms across a range of scales, including a parcellation of the cat cortex, two different parcellations of the Macaque cortex, and a representation of the nervous system of *C. elegans*, which is a tiny round worm and one of only a few organisms to date for which the entire nervous system is mapped out. All networks are available via the Brain Connectivity Toolbox [18]. Connectivity of each connectome is described by a binary connectivity matrix A, such that $a_{ij} = 1$ if brain region (neuron) i projects onto brain region (neuron) j and is otherwise zero. Note that we restrict our analysis to the giant strongly connected component of each network since this guarantees the existence of a globally synchronised state [19]. Undirected representations of each network are obtained by making all connections bidirectional resulting in a symmetric adjacency matrix given by $B = \mathrm{sgn}\left(A + A^T\right)$, where $\mathrm{sgn}(x)$ denotes the sign function. See table 1 for details of the size and density of the networks in both the directed and undirected cases.

In addition, fig. 1 shows the results of a network analysis for different connectomes using a range of standard network measures, including network density ρ; the global Watts-Strogatz clustering coefficient $\langle C \rangle$; the global efficiency ϵ; and the Newman-Girvan (NG) modularity score Q. The reader is referred to the excellent text by Newman [2] for the precise definitions of the aforementioned metrics. In general, the loss of directionality has the effect of artificially inflating network measures; local metrics such as density and clustering increase due to the inclusion of reciprocal edges, whilst network efficiency is enhanced since the additional false positive connections facilitate shorter routes within the network. In contrast, we find that network modularity decreases across all four connectomes with a smaller number of modules observed and/or a breakdown of the modularity structure (as quantified by the NG score) due to the existence of false positive connections in the undirected brain networks.

Table 1: Number of nodes N and edges m in the giant strongly connected components of the directed connectomes and their undirected representations.

Connectome	Directed		Undirected	
	N	m	N	m
Cat	52	818	52	515
Macaque	70	745	70	437
	85	2356	85	1481
C. elegans	235	1841	235	1656

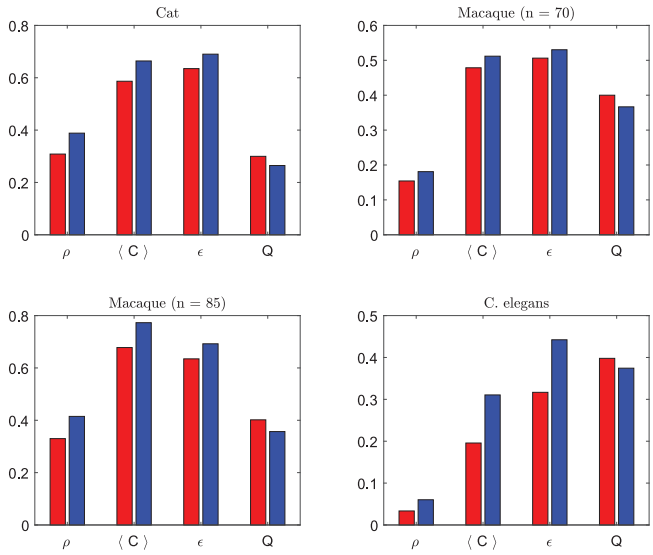

Fig. 1: Network measures for both directed (red) and undirected (blue) connectomes: ρ = density; $\langle C \rangle$ = mean clustering coefficient; ϵ = efficiency; and Q = Newman-Girvan modularity score.

Oscillator dynamics. Here, we consider N Kuramoto oscillators [20,21] whose interconnectivity is encoded by the cortical connectivity matrices defined in the previous section. The dynamical variable $\theta_i(t) \in S^1 = 2\pi\mathbb{R}/\mathbb{N}$ gives the phase of the i-th oscillator at time t. By deploying such a simple model of neural activity we aim to reveal mechanistic insights into the role that directed topology plays in neural synchrony. (See [12] for a discussion of the relationship of this model to neurobiological systems, including its inherent limitations.)

Oscillator dynamics are governed by the following set of equations:

$$\frac{\mathrm{d}\theta_i}{\mathrm{d}t} = \omega_i + S\sum_{j=1}^{N} a_{ji}\sin\left(\theta_j - \theta_i - \beta\right) \quad \text{for } i = 1, \ldots, N. \tag{1}$$

Here, S is the coupling strength, β is a phase delay term that accounts for finite signal propagation speeds, ω_i denotes the natural frequencies of the uncoupled oscillators,

and a_{ij} describes the elements of the cortical connectivity matrix as described above.

For $\beta = 0$ the system in (1) admits a fully synchronised solution of the form

$$\theta_i(t) \equiv \theta_j(t) =: \theta(t). \tag{2}$$

For non-zero values of β the solution in (2) is no longer guaranteed, rather in this case we observe either phase locked solutions such that $\theta_i - \theta_j$ is constant $\forall i, j$ or so-called cluster states in which two or more groups of synchronised oscillators coexist [19,22].

Results. – In the experiments to follow, eq. (1) was integrated from $t = 0$ to $t = 100$ using the built-in Matlab solver `ode45` with step size $\delta t = 0.01$ and absolute and relative tolerances set at 10^{-8}. In accordance with [23,24], natural frequencies of the oscillators were drawn from a Gaussian distribution with mean frequency $f = 10\,\mathrm{Hz}$ (or $\omega = f \cdot 2\pi\,\mathrm{rad/s}$) and variance one. Note that this choice of frequencies allows for ease of comparison with related work [23–25]; however, our numerical experiments suggest that for small non-zero values of the phase delay β, the results are qualitatively similar regardless of the choice of the mean natural frequency ω. To determine the dependence on initial data, each simulation was repeated 100 times with different sets of initial conditions $\theta(0)$ drawn uniformly at random form the interval $[0, 2\pi)$.

Synchronisation speed. In this section we assume identical oscillators so that $\omega_i = \omega$ and set the phase lag $\beta = 0$ thus guaranteeing the existence of the completely synchronised solution in (2). To determine the time scales of synchronisation for the different connectomes we compute the distance

$$d(t) = \max_{i,j} \mathrm{dist}\,(\theta_i, \theta_j)\,, \tag{3}$$

where

$$\mathrm{dist}\,(\theta, \theta') = \min\{|\theta - \theta'|, 2\pi - |\theta - \theta'|\} \tag{4}$$

is the circular distance between two phases θ and θ' on S^1. Note that after some initial transient, convergence to the synchronous state decays as $d(t) \sim \exp(-t/\tau)$, where τ denotes the characteristic time scale of each cortical network. Theoretically, this characteristic time scale is given by

$$\tau = -\frac{1}{\mathrm{Re}(\lambda_2)}, \tag{5}$$

where λ_2 is the second largest eigenvalue of the graph Laplacian [26], which in this case coincides with the stability matrix, or Jacobian, of (1) evaluated at the synchronous state. (See, for example, [27] for further details.)

In fig. 2 we plot the logarithm of the decaying distances for directed (red line) and undirected (blue line) representations of each of the connectomes described in table 1. In addition, we plot slopes of $-1/\tau$ for both directed (red dashed line) and undirected (blue dashed line) networks,

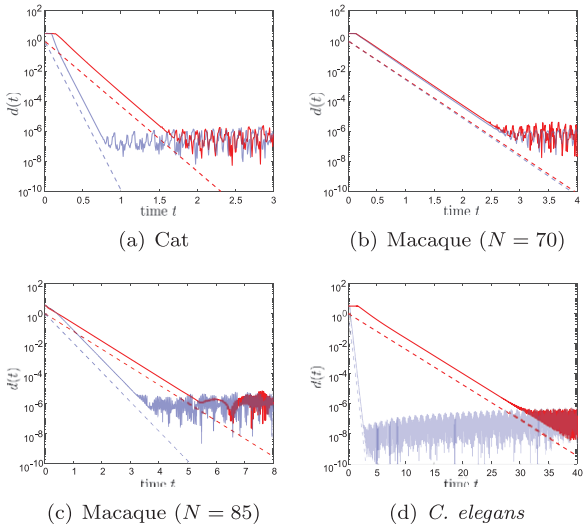

(a) Cat (b) Macaque ($N = 70$) (c) Macaque ($N = 85$) (d) *C. elegans*

Fig. 2: Time scales for synchronisation of connectome-based oscillator networks for directed (solid red line) and undirected (solid blue line) representations. Dashed lines have slope given by $-1/\tau$, where $\tau = -1/\mathrm{Re}(\lambda_2)$ is the theoretical characteristic time scale for each network and λ_2 is the second largest (in real part) eigenvalue of the associated graph Laplacian.

where τ is the theoretical time scale given in (5). Importantly, we find that in all cases synchronisation times are increased for the directed connectomes, and also, that, with the exception of the Macaque network on $N = 70$ nodes (which displays very similar time scales regardless of directionality), these differences scale with the size of the network. This result is consistent with our earlier network analysis in that the heightened efficiencies observed for the undirected networks would appear to promote faster (although likely unrealistic and undesirable biologically) synchrony propagation. We further note that the theoretical time scales predicted by (5) are in excellent agreement with the simulation results.

Stability of the phase-locked state. For non-zero β the solution in (2) is no longer guaranteed to exist; however, by introducing the following local order parameter

$$r_j e^{i\Theta_j} = \frac{1}{k_j^{\mathrm{in}}} \sum_{k=1}^{N} a_{kj} e^{i\theta_k}, \tag{6}$$

and deploying a rotating coordinate frame (*i.e.*, introducing the change of variables $\phi = \theta - \Omega t$, where Ω is the asymptotic population frequency) eq. (1) can be rewritten as

$$\frac{\mathrm{d}\phi_i}{\mathrm{d}t} = \omega_i - \Omega + S k_i^{\mathrm{in}} r_i \sin(\Phi_i - \phi_i - \beta) \quad i = 1, \ldots, N. \tag{7}$$

Here, $\Phi_i = \Theta_i - \Omega t$.

Importantly, provided $|\omega_i - \Omega| \leq S k_i^{\mathrm{in}} r_i\ \forall i$, the system in (7) exhibits a stable fixed point solution (*i.e.*, (1) has a stable phase locked solution) ϕ^* as long as the conditions

$$\cos(\Phi_i - \phi_i^* - \beta) > 0, \quad i = 1, \ldots, N \tag{8}$$

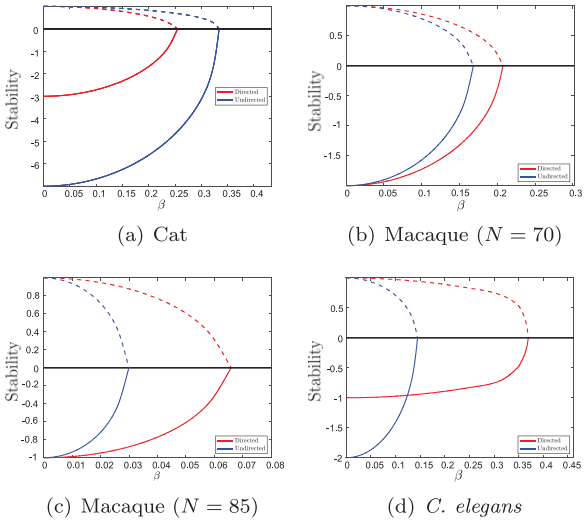

(a) Cat (b) Macaque ($N = 70$)

(c) Macaque ($N = 85$) (d) *C. elegans*

Fig. 3: Stability of the phase-locked state as a function of beta for the directed (red) and undirected (blue) connectomes displayed in table 1. Solid lines display the real part of the largest eigenvalue of the Jacobian of (7), whilst dashed lines display the value of (8) for the corresponding eigenmode.

are satisfied. To see this, note that the Jacobian matrix for the system in (7) is given by

$$J_{ij} = -Sk_i^{\text{in}} r_i \cos\left(\Phi_i - \phi_i - \beta\right) \delta_{ij}. \tag{9}$$

Here, we are assuming that r_i, Φ_i are constant $\forall i$ and δ_{ij} denotes the Kronecker delta.

Figure 3 displays stability of the phase-locked state for each of the four connectomes as a function of the phase lag variable β. Solid lines display the real part of the largest eigenvalue of the stability matrix of (7) for directed (red) and undirected (blue) connectomes, whilst dashed lines display the value of (8) for the corresponding eigenmode. We see that directionality has the general effect of increasing the robustness of the phase-locked state with all but the cat cortical network showing decreased stability in the bidirectional case. In contrast to the other connectomes studied, the addition of false positive connections (that arise when directionality is neglected) in the cat connectome significantly elevates the minimal in-degree (from 3 to 7 as can be seen in fig. 3(a)), which has a positive stabilising effect on the fully synchronised (*i.e.*, $\beta = 0$) solution. This follows since for $\beta = 0$ the Jacobian matrix in (9) reduces to $J_{ij} = -Sk_i^{\text{in}}\delta_{ij}$. Thus, whilst we observed increased decay rates (as a function of β) of the eigenmodes across all undirected network representations, the undue elevation of the stability properties for the cat connectome enhances its robustness relative to the directed connectome. For values of β outside of these ranges partially locked states can be observed in which a subset of nodes are phase locked whilst the remaining nodes drift monotonically.

Phase lag/lead relationships. The relationship between local dynamics, phase and network structure has recently received considerable interest [23–25] due to the significant role of neural oscillations in healthy brain function. Deploying *directed phase lag index* (dPLI) [28] as a measure of directed functional (or *effective*) connectivity, the authors of [23,24] found that network degree was an excellent predictor of the type of directed functional connectivity patterns typically observed experimentally in undirected connectomes. Here, we deploy dPLI to investigate the extent to which directed structural topology impacts phase relationships between signals from distant brain areas.

For a given node pair, dPLI is measured as

$$\text{dPLI}_{ij} = \langle \text{sgn}\left(\Delta\theta_{ij}(t)\right)\rangle, \tag{10}$$

where $\Delta\theta_{ij}(t) = \theta_i(t) - \theta_j(t)$ denotes the instantaneous phase difference between nodes i and j; the sign function yields 1 if $\Delta\theta_{ij}(t) > 0$, 0 if $\Delta\theta_{ij}(t) = 0$ and -1 if $\Delta\theta_{ij}(t) < 0$; and angled brackets denotes a time average. The range of dPLI is $[-1, 1]$. If a node leads on average then it obtains a dPLI score in $(0, 1]$; if it lags on average a score in $[-1, 0)$ and a score of zero in the absence of a phase-lead/lag relationship [28].

For sufficiently small positive values of β (*i.e.*, such that the phase-locked solution of (1) exists) we have the following analytic expression for the asymptotic phases:

$$\phi_i^* = \sin^{-1}\left(\frac{\omega_i - \Omega}{Sk_i^{\text{in}} r_i}\right) + \Phi_i - \beta, \quad i = 1, \ldots, N, \tag{11}$$

which results from solving the right-hand side of (7) set equal to zero. From the above we see that the phase dynamics depend on both the in-degree and the local order parameter given in (6); in [23,24] it was shown experimentally that an inverse relationship between node degree and phase (as measured using dPLI) exists for undirected large-scale connectomes, that is, that the effect of the local order parameter was largely negligible. In our experiments, we found a similar result held for the large-scale connectomes in both directed and undirected representations, although the correlations were weaker in the directed representations (see the Supplementary Material `Supplementarymaterial.pdf`). However, in the case of the invertebrate *C. elegans* connectome, we found evidence suggesting a breakdown in these relations at this scale for the directed network.

Figure 4(a) displays simulation results in which eq. (1) is solved numerically for both directed (top) and undirected (bottom) representations of the *C. elegans* connectome. In these experiments we set the coupling strength $S = 1$ and the phase delay $\beta = 0.1$. A snapshot of the Kuramoto model in action at time $t = 100$ is plotted on the unit circle for both networks (left), as well as a plot of the relative phase ϕ against time (right). In addition, in each plot we highlight in yellow the five nodes with lowest degree and in green the five nodes with highest degree. In the case of the undirected network, we observe, in accordance with [23,24], a clear relationship between phase

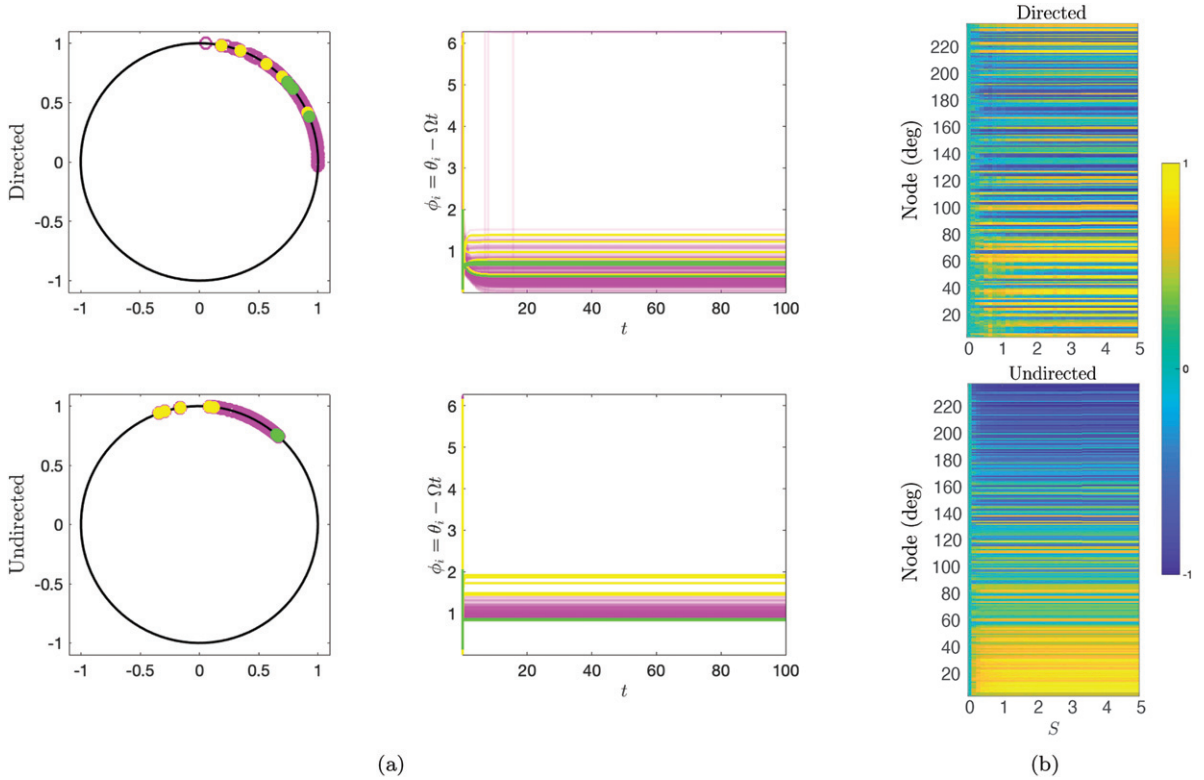

Fig. 4: Numerical simulations with $\beta = 0.1$ for the *C. elegans* connectome for both directed (top) and undirected (bottom) representations. (a) Snapshot ($t = 100$) of the phase dynamics ($S = 1$) plotted on the unit circle (left) and relative phase, ϕ, *vs.* time, t (right). (b) dPLI as a function of coupling strength S.

and node degree: low-degree nodes phase lead whist high-degree nodes phase lag. For the directed network no such relation is evident, rather low- and high-degree nodes are interspersed amongst nodes of varying degree. Moreover, it is evident from fig. 4(b), where we display mean dPLI (*i.e.*, $\langle \mathrm{dPLI}_{ij} \rangle_j$) of each node arranged in ascending order of its in-degree for coupling values, S, ranging from zero to five, that the aforementioned patterns prevail under variation of the coupling strength S. Importantly, this result implicates a potentially distinctive role for directed network topology in determining the nature of synchronous neural activity at different scales within the brain.

Conclusion. – In this letter, we have investigated the impact that network directionality has on the synchronisation dynamics of neural activity in connectome networks. Deploying a Kuramoto phase model of neural dynamics, we performed numerical simulations to probe important properties of neural synchrony, such as synchronisation times, the impact of neural delays and the role of directionality in determining phase relationships between distant brain regions. The Kuramoto model is a highly simplified model with which to investigate synchrony properties in directed connectomes; indeed, several features of relevance such as complex node dynamics, stochasticity or distance-dependent coupling and/or delays, are omitted from our formulation; however, such an approach allows us to provide a more powerful exposition of the importance of network structure imparted by the directed cortical topology, in isolation.

Our results are significant for a number of reasons. First, they demonstrate how perturbing the directed topology (*i.e.*, via the inclusion of false positive connections inherent in generating undirected representations of the connectome) can significantly impact both synchonisation times and robustness properties of synchonised and phase-locked states. We found that undirected networks synchronise faster but are less robust to the inclusion of time delays, thus suggesting network directionality as a potential candidate mechanism for regulating spreading dynamics within the brain. Second, our study suggests that recent developments (see, for example, [23,24]) highlighting relations between network degree and functional directionality patterns, whilst remaining consistent across directed large-scale connectomes, appear to break down for micro-scale neuroarchitectures such as the *C. elegans* connectome. These results are likely a manifestation of observed differences between motif and community network structures (see, for example, [29,30] and references therein) that exist for the different species considered here, and which have recently been hypothesised to underpin phase-synchrony in large-scale brain networks [31].

The focus of future work shall be twofold: i) investigate how the results obtained in this study are altered when

deploying a signal transition model which more accurately reflects the behaviour of a neural unit (brain region or neuron depending upon the scale); and ii) consider other micro-scale architectures (*e.g.*, drosophila and mouse connectomes) to determine the extent to which macro- and micro-scale networks can be characterised by their synchrony properties.

* * *

AP would like to acknowledge Nottingham Trent University for funding via a Vice-Chancellor's PhD Scholarship. This is internal University funding and so no funding body or associated grant number exists; however, we would still like to acknowledge this support.

Data availability statement: No new data were created or analysed in this study.

REFERENCES

[1] Estrada E., *The Structure of Complex Networks: Theory and Applications* (Oxford University Press) 2012.
[2] Newman M., *Networks* (Oxford University Press) 2018.
[3] Winfree A. T., *The Geometry of Biological Time*, Vol. **12** (Springer Science & Business Media) 2001.
[4] Pikovsky A., Kurths J., Rosenblum M. and Kurths J., *Synchronization: A Universal Concept in Nonlinear Sciences*, No. 12 (Cambridge University Press) 2003.
[5] van Wijk B., Beek P. J. and Daffertshofer A., *Front. Hum. Neurosci.*, **6** (2012) 252.
[6] Swann N. C., de Hemptinne C., Aron A. R., Ostrem J. L., Knight R. T. and Starr P. A., *Ann. Neurol.*, **78** (2015) 742.
[7] Percha B., Dzakpasu R., Żochowski M. and Parent J., *Phys. Rev. E*, **72** (2005) 031909.
[8] Fries P., *Trends Cognit. Sci.*, **9** (2005) 474.
[9] Wang H. E., Bénar C. G., Quilichini P. P., Friston K. J., Jirsa V. K. and Bernard C., *Front. Neurosci.*, **8** (2014) 405.
[10] Cumin D. and Unsworth C., *Phys. D: Nonlinear Phenom.*, **226** (2007) 181.
[11] Cabral J., Hugues E., Sporns O. and Deco G., *Neuroimage*, **57** (2011) 130.
[12] Breakspear M., Heitmann S. and Daffertshofer A., *Front. Hum. Neurosci.*, **4** (2010) 190.
[13] Forrester M., Crofts J. J., Sotiropoulos S. N., Coombes S. and O'Dea R. D., *Netw. Neurosci.*, **4** (2020) 467.
[14] Asllani M., Challenger J. D., Pavone F. S., Sacconi L. and Fanelli D., *Nat. Commun.*, **5** (2014) 1.
[15] Padmore A., Nelson M. R., Chuzhanova N. and Crofts J. J., *J. Complex Netw.*, **8** (2020) cnaa033.
[16] Hoppensteadt F. C. and Izhikevich E. M., *Weakly Connected Neural Networks*, Vol. **126** (Springer Science & Business Media) 2012.
[17] Varela F., Lachaux J.-P., Rodriguez E. and Martinerie J., *Nat. Rev. Neurosci.*, **2** (2001) 229.
[18] Rubinov M. and Sporns O., *Neuroimage*, **52** (2010) 1059.
[19] Restrepo J. G., Ott E. and Hunt B. R., *Chaos*, **16** (2006) 015107.
[20] Dörfler F. and Bullo F., *Automatica*, **50** (2014) 1539.
[21] Rodrigues F. A., Peron T. K. D., Ji P. and Kurths J., *Phys. Rep.*, **610** (2016) 1.
[22] Strogatz S. H., *Phys. D: Nonlinear Phenom.*, **143** (2000) 1.
[23] Moon J.-Y., Lee U., Blain-Moraes S. and Mashour G. A., *PLoS Comput. Biol.*, **11** (2015) e1004225.
[24] Moon J.-Y., Kim J., Ko T.-W., Kim M., Iturria-Medina Y., Choi J.-H., Lee J., Mashour G. A. and Lee U., *Sci. Rep.*, **7** (2017) 1.
[25] Petkoski S., Palva J. M. and Jirsa V. K., *PLOS Comput. Biol.*, **14** (2018) e1006160.
[26] Merris R., *Linear Algebra Appl.*, **197** (1994) 143.
[27] Grabow C., Grosskinsky S. and Timme M., *Eur. Phys. J. B*, **84** (2011) 613.
[28] Stam C. J. and van Straaten E. C., *Neuroimage*, **62** (2012) 1415.
[29] Sporns O., Kötter R. and Friston K. J., *PLoS Biol.*, **2** (2004) e369.
[30] van den Heuvel M. P. and Yeo B. T., *Neuron*, **93** (2017) 1248.
[31] Gollo L. L. and Breakspear M., *Philos. Trans. R. Soc. B: Biol. Sci.*, **369** (2014) 20130532.